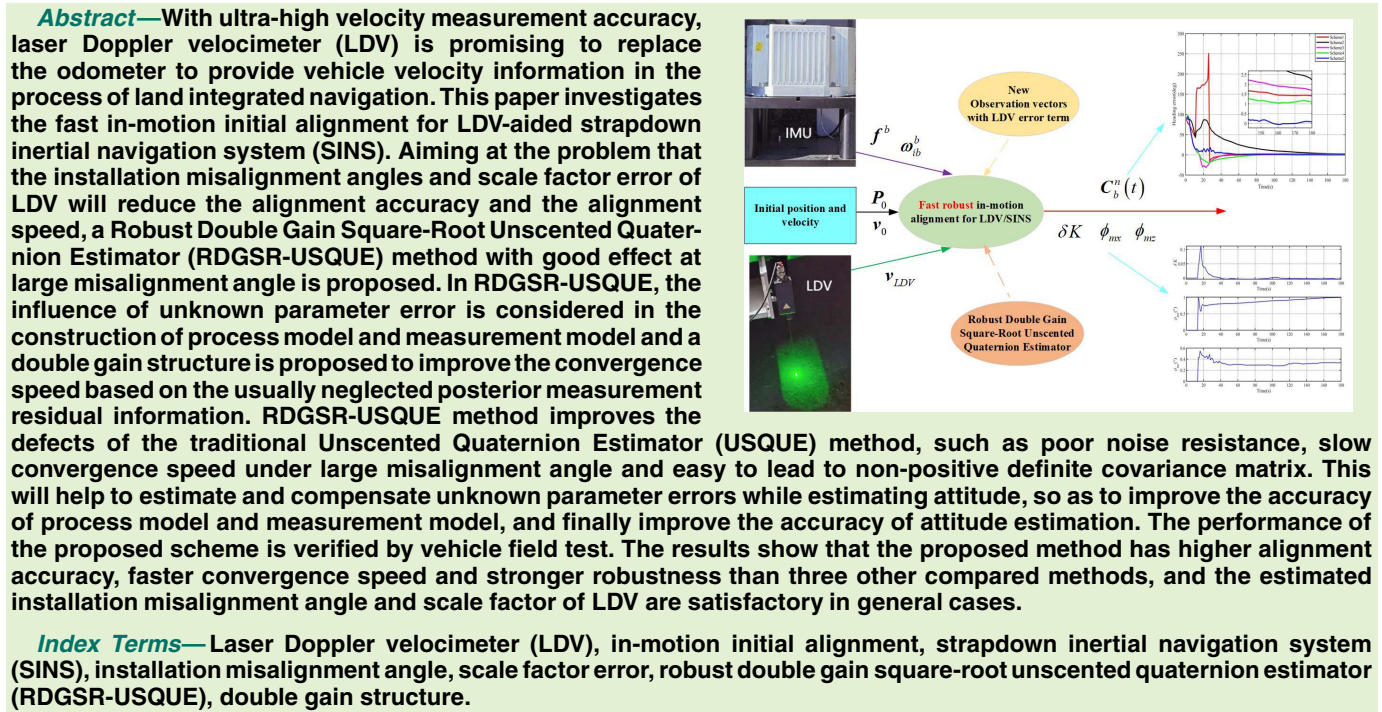


A Fast Robust In-Motion Alignment Method for Laser Doppler Velocimeter-Aided Strapdown Inertial Navigation System

Zhiyi Xiang^{ID}, Qi Wang, Rong Huang, Chongbin Xi, Xiaoming Nie, and Jian Zhou^{ID}



I. INTRODUCTION

STRAPDOWN inertial navigation system (SINS) has been widely used in military, industrial and consumer fields because of its self-containment, anti-jamming capability, high sampling rate and good concealment. The SINS determines the navigation parameters of the vehicle according to the outputs

Manuscript received 10 January 2022; revised 25 June 2022; accepted 12 July 2022. Date of publication 26 July 2022; date of current version 1 September 2022. This work was supported in part by the Major Basic Autonomous Research Project of the College of Advanced Interdisciplinary Studies, National University of Defense Technology, under Grant ZDJC19-12 and in part by the Natural Science Foundation of Hunan Province, China, under Grant 2021JJ30782. The associate editor coordinating the review of this article and approving it for publication was Dr. Tania Dutta. (*Corresponding author: Jian Zhou*)

The authors are with the College of Advanced Interdisciplinary Studies, National University of Defense Technology, Changsha 410073, China (e-mail: xiangzhiyi0816@gmail.com; tianmawangqi@hotmail.com; huangrong_nudt@163.com; xichongbin@nudt.edu.cn; thudpm@gmail.com; wttzhoujian@163.com).

Digital Object Identifier 10.1109/JSEN.2022.3191120

of accelerometers and gyroscopes. However, due to the initial alignment error and inertial sensors errors, the positioning error of SINS will accumulate along with the time. As a result, the initial alignment with high accuracy and rapidness and sensors with little measurement error are essential to guarantee long-term performance of SINS [1]–[3]. The initial alignment mainly refers to the determination of initial attitude, which determines the attitude matrix between the body frame and the navigation frame. Compared with the traditional static-base alignment, in-motion alignment can greatly improve the mobility of the vehicle, which is an advantageous functionality in military applications [4], [5]. When the vehicle is running, it is difficult to obtain the accurate gravity information of the vehicle in the inertial frame due to the acceleration of the vehicle to the ground. Under this circumstance, it is impossible to complete the accurate autonomous initial alignment process only relying on the measurement of the gyroscope and accelerometer of the SINS.

To implement the in-motion initial alignment procedure efficiently, much effort has been devoted to investigating the novel alignment methods. An optimization-based alignment (OBA) method was proposed for GPS-aided high-accuracy SINS. In the OBA method, the attitude matrix is decomposed into two time-varying attitude matrices and a constant attitude matrix. The two time-varying attitude matrices are calculated by the body angular rate and the navigation angular rate respectively. Finally, the constant attitude matrix is obtained based on the constructed vector observations using Davenport's q-method [6], [7]. After that, many OBA methods have been proposed for GPS-aided SINS, such as velocity/ position integration-based OBA method [8], velocity-based OBA method [9], position loci-based OBA method [10] and sliding- window-based OBA method [11], [12]. The OBA method has been considered as a promising method for high-accuracy SINS due to its fastness and anti-jamming capability. To extend the application, the OBA methods aided by ground velocity in the body frame have been derived and applied to odometer (OD) and Doppler Velocity Log (DVL) in [13], [14]. However, most of the existing OBA methods do not take the inertial measurement unit (IMU) bias into account and OBA methods cannot estimate other error parameters except attitude, which will affect the accuracy of the constructed vector observations. Therefore, the OBA method is not applicable to low-cost SINS. In order to improve the accuracy of OBA methods, an in-motion initial alignment method based on Kalman filter is proposed on the basis of OBA method [15], [16]. For large initial alignment error, the unscented-transformation-based unscented Kalman filter (UKF) is used for in-motion initial alignment because of its easy implementation, moderate computational cost and appropriate performance [17]. The UKF in its quaternion application form is proposed to avoid the singularity problem and the norm constraint of the quaternion in practical applications, called Unscented Quaternion Estimator (USQUE)[18]. The USQUE is approved as a method that can replace OBA method due to its capability of estimating other parameters other than the attitude and handing the noise in the model. In order to achieve the in-motion initial alignment for low-cost SINS, a new OBA method based on dynamic attitude estimation technique was proposed, which can jointly estimate the time-varying attitude matrix from current body frame to initial body frame and gyroscope bias by using USQUE [19]. For high-accuracy SINS, an alignment method based on attitude estimation was proposed by using USQUE to weaken the interference of odometer [20]. In a DVL-aided initial alignment scheme, USQUE is employed to perform the fine alignment process after the OBA method [21]. Unfortunately, USQUE converges slowly under large unknown initial attitude error. As a variant of UKF, it lacks adaptive ability to system noise and easily leads to non-positive definite covariance matrix. In [22] and [23], the group of double direct spatial isometries is used for initial alignment, but the comparison with the mainstream alignment scheme is not given. In addition, in order to further improve the accuracy of the alignment, the fine alignment process can be continued, and the sensor error can be taken into account in the fine alignment process [21], [24].

However, in most cases, in-motion fine alignment is regarded as a part of the subsequent integrated navigation process, because when the attitude error is small, the in-motion fine alignment algorithm and the integrated navigation algorithm can be considered as no different.

As a new type of velocity sensor, laser Doppler velocimeter (LDV) has the advantages of high accuracy, rapid dynamic response, non-contact measurement, good directional sensitivity, complete autonomy and good spatial resolution. Our research group has proposed a variety of LDV structures to measure true vehicle velocity over ground, and have a higher velocity measurement accuracy than OD and DVL [25]–[30]. At present, there are few reports about the application of LDV in the field of navigation. In this paper, a new LDV-aided in-motion initial alignment method is proposed, named Robust Double Gain Square-Root Unscented Quaternion Estimator (RDGSUR-USQUE).

The contributions of proposed in-motion alignment method are listed hereafter:

(1) This paper improves the process model and measurement model constructed in literature [20], a more accurate process model and measurement model for LDV-aided SINS in-motion alignment is derived, which takes into account the installation misalignment angle, scale coefficient of LDV and the ignored small quantity related to earth rotation rate in body frame.

(2) In order to ensure the stability of numerical values and the positive definiteness of covariance matrix, square root optimization is carried out on the basis of traditional USQUE algorithm.

(3) Adaptive processing of measurement noise covariance matrix makes the filter always keep good performance without divergence and accelerate the convergence of the attitude error.

(4) In order to improve the in-motion alignment speed, a double gain structure is proposed based on the posterior measurement residual information which is usually neglected.

The rest of this paper is organized as follows. In Section II, the vector observations of the proposed scheme are deduced mathematically, and the process model and observation model are established. In Section III, a more stable RDGSUR-USQUE method is proposed. In Section IV, the proposed method is compared with the existing typical methods by using the vehicle-mounted field test data collected from LDV-aided laser SINS. Concluding remarks are given in Section V.

II. IN-MOTION ALIGNMENT FOR SINS/LDV

In this paper, some important coordinate systems are usually involved, including the local level navigation frame (n -frame), the SINS body frame (b -frame), the inertial nonrotating frames (i -frame), the earth frame (e -frame) and the LDV's frame (m -frame). The purpose of SINS initial alignment is to determine the matrix C_b^n , which is the attitude matrix from the b -frame to the n -frame. In order to further improve the accuracy of alignment, it is necessary to estimate the matrix C_m^b , which is the installation misalignment matrix of m -frame with respect to b -frame.

The velocity kinematic equation in the n -frame is known as

$$\dot{\mathbf{v}}^n = C_b^n \mathbf{f}^b - (2\omega_{ie}^n + \boldsymbol{\omega}_{en}^n) \times \mathbf{v}^n + \mathbf{g}^n \quad (1)$$

where \mathbf{v}^n represents the ground velocity expressed in the n -frame, \mathbf{f}^b denotes the specific force in b -frame, \mathbf{g}^n is the gravity vector in n -frame, $(\cdot) \times$ means to solve the antisymmetric matrix, $\boldsymbol{\omega}_{ie}^n$ represents the earth rotation rate, and $\boldsymbol{\omega}_{en}^n$ is the navigational rotating rate in n -frame relative to e -frame. The $\boldsymbol{\omega}_{ie}^n$ and $\boldsymbol{\omega}_{en}^n$ can be expressed, respectively, as

$$\boldsymbol{\omega}_{ie}^n = [0, \omega_{ie} \cos L, \omega_{ie} \sin L]^T \quad (2)$$

$$\boldsymbol{\omega}_{en}^n = [-\frac{v_N^n}{R_M + h}, \frac{v_E^n}{R_N + h}, \frac{v_E^n}{R_N + h} \tan L]^T \quad (3)$$

where L is the local latitude, and h is altitude of the vehicle. R_M and R_N are the principal radius of curvature of the prime meridian and the equator, respectively. v_E^n is the East velocity and v_N^n is the North velocity.

The ground velocity in the n -frame can be expressed by the ground velocity in the b -frame as

$$\mathbf{v}^n = \mathbf{C}_b^n \mathbf{v}^b \quad (4)$$

By calculating the derivative of (4) and considering the formula $\dot{\mathbf{C}}_b^n = \mathbf{C}_b^n \boldsymbol{\omega}_{nb}^b (\times)$, we have

$$\dot{\mathbf{v}}^n = \mathbf{C}_b^n (\dot{\mathbf{v}}^b + \boldsymbol{\omega}_{nb}^b \times \mathbf{v}^b) \quad (5)$$

By substituting (5) into (1) and rearranging the equations, we can get

$$\mathbf{C}_b^n (\dot{\mathbf{v}}^b + (\boldsymbol{\omega}_{ib}^b + \boldsymbol{\omega}_{ie}^b) \times \mathbf{v}^b - \mathbf{f}^b) = \mathbf{g}^n \quad (6)$$

A. Process Model

According to the chain rule of direction cosine matrix, the attitude matrix $\mathbf{C}_b^n(t)$ can be expressed as

$$\mathbf{C}_b^n(t) = \mathbf{C}_{n(0)}^{n(t)} \mathbf{C}_{b(0)}^{b(0)} \mathbf{C}_{b(t)}^{b(0)} \quad (7)$$

where $\mathbf{C}_{b(0)}^{b(0)}$ is the constant attitude matrix from initial b -frame to initial n -frame. $b(0)$ and $n(0)$ denotes the initial b -frame and n -frame respectively, which both are non-rotating orthogonal frame with respect to i -frame.

According to [20], the attitude update equation can be written as

$$\dot{\mathbf{C}}_{b(t)}^i = \mathbf{C}_{b(t)}^i (\boldsymbol{\omega}_{ib}^b \times) \quad (8)$$

$$\dot{\mathbf{C}}_{n(t)}^i = \mathbf{C}_{n(t)}^i (\boldsymbol{\omega}_{in}^n \times) \quad (9)$$

Equation (9) is the process model.

B. Measurement Model

Substitute (7) into (6) and multiply $\mathbf{C}_{n(t)}^i$ on both sides to get the following formula

$$\mathbf{C}_{b(t)}^i (\dot{\mathbf{v}}^b + (\boldsymbol{\omega}_{ie}^b + \boldsymbol{\omega}_{ib}^b) \times \mathbf{v}^b - \mathbf{f}^b) = \mathbf{C}_{n(t)}^i \mathbf{g}^n \quad (10)$$

Integral in the time interval of interest on both sides of (10), it can be obtained that

$$\int_0^t \mathbf{C}_{b(\tau)}^i (\dot{\mathbf{v}}^b + (\boldsymbol{\omega}_{ie}^b + \boldsymbol{\omega}_{ib}^b) \times \mathbf{v}^b - \mathbf{f}^b) d\tau = \int_0^t \mathbf{C}_{n(\tau)}^i \mathbf{g}^n d\tau \quad (11)$$

By the partial integration, the $\int_0^t \mathbf{C}_{b(\tau)}^i \dot{\mathbf{v}}^b d\tau$ can be expressed as

$$\begin{aligned} \int_0^t \mathbf{C}_{b(\tau)}^i \dot{\mathbf{v}}^b d\tau &= \mathbf{C}_{b(\tau)}^i \mathbf{v}^b \Big|_0^t - \int_0^t \mathbf{C}_{b(\tau)}^i (\boldsymbol{\omega}_{ib}^b) \times \mathbf{v}^b d\tau \\ &= \mathbf{C}_{b(t)}^i \mathbf{v}^b(t) - \mathbf{v}^b(0) - \int_0^t \mathbf{C}_{b(\tau)}^i (\boldsymbol{\omega}_{ib}^b) \times \mathbf{v}^b d\tau \end{aligned} \quad (12)$$

Then, substituting (12) into (11), the (11) can be expressed as

$$\begin{aligned} &\mathbf{C}_{b(t)}^i \mathbf{v}^b(t) - \mathbf{v}^b(0) + \int_0^t \mathbf{C}_{b(\tau)}^i (\boldsymbol{\omega}_{ie}^b \times \mathbf{v}^b) d\tau \\ &- \int_0^t \mathbf{C}_{b(\tau)}^i \mathbf{f}^b d\tau \\ &= \mathbf{C}_{n(t)}^i \mathbf{C}_{n(0)}^{n(t)} \int_0^t \mathbf{C}_{n(\tau)}^n \mathbf{g}^n d\tau \end{aligned} \quad (13)$$

Define two vectors as

$$\begin{cases} \boldsymbol{\alpha}(t) = \mathbf{C}_{b(t)}^i \mathbf{v}^b(t) - \mathbf{v}^b(0) + \int_0^t \mathbf{C}_{b(\tau)}^i (\boldsymbol{\omega}_{ie}^b \times \mathbf{v}^b) d\tau \\ - \int_0^t \mathbf{C}_{b(\tau)}^i \mathbf{f}^b d\tau \\ \boldsymbol{\beta}(t) = \mathbf{C}_{n(0)}^{n(t)} \int_0^t \mathbf{C}_{n(\tau)}^n \mathbf{g}^n d\tau \end{cases} \quad (14)$$

The measurement model can be given by

$$\boldsymbol{\alpha}(t) = \mathbf{C}_{n(t)}^i \boldsymbol{\beta}(t) \quad (15)$$

C. New Process Model and Measurement Model

It can be seen from (9) and (14) that the accuracy of \mathbf{v}^b will affect the alignment accuracy, where \mathbf{v}^b is regarded as the velocity provided by LDV. In order to further improve the alignment accuracy, it is necessary to consider the installation misalignment matrix (\mathbf{C}_m^b) and scale factor error (δK) of LDV. The installation misalignment angle vector is regarded as a small angle vector $\boldsymbol{\phi}_m$ in this paper. It can be seen from [31] that the roll angle does not affect the velocity measurement value of LDV. Considering that the installation position of LDV is close to IMU, the influence of lever arm effect is ignored in this paper. The \mathbf{v}^b can be expressed as

$$\mathbf{v}^b = \mathbf{C}_m^b \tilde{\mathbf{v}}^m = (\mathbf{I}_3 - \boldsymbol{\phi}_m \times) (1 + \delta K) \mathbf{v}^m \quad (16)$$

where $\boldsymbol{\phi}_m = [\phi_{mx} \ 0 \ \phi_{mz}]^T$, $\mathbf{C}_m^b = \mathbf{I}_3 - \boldsymbol{\phi}_m \times$, \mathbf{v}^m is the theoretical output of LDV. $\tilde{\mathbf{v}}^m$ is the LDV output with scale factor error. \mathbf{I}_3 is the 3×3 identity matrix, ϕ_{mx} is the pitch angle between b -frame and m -frame, and ϕ_{mz} is the heading angle error between b -frame and m -frame.

Considering the LDV scale coefficient and installation misalignment angles, a new measurement model for the matrix $\mathbf{C}_{n(t)}^i$ and a new process model can be formulated by

$$\boldsymbol{\alpha}_m(t) = \mathbf{C}_{n(t)}^i \boldsymbol{\beta}_m(t) \quad (17)$$

$$\begin{aligned} \dot{\mathbf{C}}_{n(t)}^i &= \mathbf{C}_{n(t)}^i (\boldsymbol{\omega}_{in}^n \times) \\ &= \mathbf{C}_{n(t)}^i [(\boldsymbol{\omega}_{ie}^n + \boldsymbol{\omega}_{en}^n) \times] \\ &= \mathbf{C}_{n(t)}^i \{[\boldsymbol{\omega}_{ie}^n + \mathbf{C}_b^n(t-1) \mathbf{F}_c \mathbf{v}^b] \times\} \\ &= \mathbf{C}_{n(t)}^i \{[\boldsymbol{\omega}_{ie}^n + \mathbf{C}_b^n(t-1) \mathbf{F}_c \\ &\quad \times (\mathbf{I}_3 - \boldsymbol{\phi}_m \times) (1 + \delta K) \mathbf{v}^m] \times\} \end{aligned} \quad (18)$$

where

$$\mathbf{F}_c = \begin{bmatrix} 0 & -1/(R_M + h) & 0 \\ 1/(R_N + h) & 0 & 0 \\ (\tan L)/(R_N + h) & 0 & 0 \end{bmatrix} \quad (19)$$

The first integral in (14) can be calculated as

$$\begin{aligned} & \int_0^t \mathbf{C}_{b(\tau)}^i (\boldsymbol{\omega}_{ie}^b \times \mathbf{v}^b) d\tau \\ &= \sum_{k=0}^{M-1} \mathbf{C}_{b(t_k)}^i \mathbf{C}_{n(t_k)}^{b(t_k)} \int_{t_k}^{t_{k+1}} \mathbf{C}_{n(\tau)}^{n(t_k)} (\boldsymbol{\omega}_{ie}^n \times) \mathbf{v}^n(\tau) d\tau \end{aligned} \quad (20)$$

where $t = MT$, t is current time instant during the in-motion alignment, T is the sampling interval of the SINS and LDV. LDV has the same sampling frequency as SINS, which GPS and DVL do not possess.

According to [8], the incremental integral in (20) can be approximated by

$$\begin{aligned} \Delta \mathbf{v}^{n(t_k)} &= \int_{t_k}^{t_{k+1}} \mathbf{C}_{n(\tau)}^{n(t_k)} (\boldsymbol{\omega}_{ie}^n \times) \mathbf{v}^n(\tau) d\tau \\ &= \left(\frac{T}{2} \mathbf{I}_3 + \frac{T^2}{6} \boldsymbol{\omega}_{in}^n \times \right) \boldsymbol{\omega}_{ie}^n \times \mathbf{v}^n(t_k) \\ &\quad + \left(\frac{T}{2} \mathbf{I}_3 + \frac{T^2}{3} \boldsymbol{\omega}_{in}^n \times \right) \boldsymbol{\omega}_{ie}^n \times \mathbf{v}^n(t_{k+1}) \end{aligned} \quad (21)$$

The second integral in (14) can be calculated as

$$\int_0^t \mathbf{C}_{b(\tau)}^i f^b d\tau = \sum_{k=0}^{M-1} \mathbf{C}_{b(t_k)}^i \int_{t_k}^{t_{k+1}} \mathbf{C}_{b(\tau)}^{b(t_k)} f^b(\tau) d\tau \quad (22)$$

According to [8], two-sample correction is used to approximate the incremental integral in (22).

$$\begin{aligned} \Delta \mathbf{v}^{b(t_k)} &= \int_{t_k}^{t_{k+1}} \mathbf{C}_{b(\tau)}^{b(t_k)} f^b(\tau) d\tau \\ &= \Delta \mathbf{v}_1 + \Delta \mathbf{v}_2 + \frac{1}{2} (\Delta \boldsymbol{\theta}_1 + \Delta \boldsymbol{\theta}_2) \times (\Delta \mathbf{v}_1 + \Delta \mathbf{v}_2) \\ &\quad + \frac{2}{3} (\Delta \boldsymbol{\theta}_1 \times \Delta \mathbf{v}_2 + \Delta \mathbf{v}_1 \times \Delta \boldsymbol{\theta}_2) \end{aligned} \quad (23)$$

The vector $\boldsymbol{\alpha}_m(t)$ and $\boldsymbol{\beta}_m(t)$ from (17) are given by

$$\begin{cases} \boldsymbol{\alpha}_m(t) = \mathbf{C}_{b(t_M)}^i (\mathbf{I}_3 - \boldsymbol{\phi}_m \times) (1 + \delta K) \mathbf{v}^m(t_M) \\ \quad - (\mathbf{I}_3 - \boldsymbol{\phi}_m \times) (1 + \delta K) \mathbf{v}^m(0) \\ \quad + \sum_{k=0}^{M-1} \mathbf{C}_{b(t_k)}^i \mathbf{C}_{n(t_k)}^{b(t_k)} \Delta \mathbf{v}^{n(t_k)} - \sum_{k=0}^{M-1} \mathbf{C}_{b(t_k)}^i \Delta \mathbf{v}^{b(t_k)} \\ \boldsymbol{\beta}_m(t) = \mathbf{C}_{n(0)}^{n(t_M)} \sum_{k=0}^{M-1} \mathbf{C}_{n(t_k)}^{n(0)} \left(T \mathbf{I}_3 + \frac{T^2}{2} \boldsymbol{\omega}_{in}^n \times \right) \mathbf{g}^n(t_k) \end{cases} \quad (24)$$

where T is the sampling interval.

III. PROPOSED ROBUST DOUBLE GAIN SQUARE-ROOT UNSCENTED QUATERNION ESTIMATOR ALGORITHM

The mainstream OBA method cannot estimate $\mathbf{C}_{n(t)}^i$, $\boldsymbol{\phi}_m$ and δK effectively. USQUE is a method based on attitude estimation, which can estimate the above parameters. However, as a quaternion application form of UKF, USQUE has the following drawbacks: firstly, its convergence speed is slower

than OBA method; secondly, it lacks the self-adaptive capacity to deal with system noise; finally, it is easy to cause the matrix nonpositive definiteness. In order to solve the above defects, the square root and robust optimization are carried out for the traditional USQUE in this section, and the double gain structure is applied in USQUE, the new method is called RDGSR-USQUE. Equation (18) and (17) is the continuous process and measurement model.

In navigation calculation, the directional cosine matrix needs to use 9 parameters and the quaternion and Euler angles only needs 4 parameters and 3 parameters. Although Euler angles only needs three parameters, Gimbal Lock is an inevitable problem of Euler angle, so the quaternion has been often used to represent attitude in navigation calculation. The direct implementation of a UKF with quaternion-based state is not suitable because the quaternion estimate is determined using the weighted quaternions averaging operation. Thus, no guarantees can be made that the quaternion will have unit norm. To represent an attitude-error quaternion preserving the constraint of quaternion propagation, the quaternion is used for attitude propagation and the unconstrained three-component vectors of generalized Rodrigues parameters (GRP) are used for filtering and local attitude error representation [18], [32]–[34].

In RSRUSQUE, the filtering state is defined as

$$\hat{\mathbf{X}}_k = \left[\delta \mathfrak{R}_k^T \hat{\mathbf{X}}_k^{eT} \right]^T \quad (25)$$

where $\delta \mathfrak{R}_k$ is the corresponding GRP representation about the attitude error quaternion $\delta \mathbf{q}_n^i$, and the $\delta \mathbf{q}_n^i$ denotes the error between the n -frame and the i -frame. $\hat{\mathbf{X}}_k^e$ is the components of the state besides the quaternion. For the proposed initial alignment model, it is

$$\hat{\mathbf{X}}_k^e = [\phi_{mx} \phi_{mz} \delta K]^T \quad (26)$$

Due to the attitude error is represented by GRP in the filtering state and represented by quaternion in the attitude propagation process. Therefore, in the RDGSR-USQUE, quaternion and their corresponding GRP representation should be converted to each other to ensure the normal filtering process. The inverse transformation from $\delta \mathbf{q}$ to $\delta \mathfrak{R}$ is given by

$$\delta \mathfrak{R} = f \frac{\delta \boldsymbol{\rho}}{a + \delta q_0} \quad (27)$$

where a is a parameter from 0 to 1 and f is a scale factor. The generalized Rodrigues parameters are used to place the singularity of the attitude representation in a certain angle range. Different combinations of a and f have different physical meanings. For instance, when $a = 0$ and $f = 1$, (27) gives the Gibbs vector, and when $a = f = 1$, (27) gives the standard vector of modified Rodrigues parameters. $\delta \mathbf{q} = [\delta q_0, \delta \mathbf{q}_{1:3}^T]^T = [\delta q_0, \delta \boldsymbol{\rho}^T]^T$ is the attitude error quaternion.

The inverse transformation from $\delta \mathfrak{R}$ to $\delta \mathbf{q}$ is given by

$$\begin{cases} \delta q_0 = \frac{-a \|\delta \mathfrak{R}\|^2 + f \sqrt{f^2 + (1-a^2) \|\delta \mathfrak{R}\|^2}}{f^2 + \|\delta \mathfrak{R}\|^2} \\ \delta \boldsymbol{\rho} = f^{-1} (a + \delta q_0) \delta \mathfrak{R} \end{cases} \quad (28)$$

Since the attitude is updated in the form of quaternion during alignment, the process model (18) is converted to the following quaternion form.

$$\mathbf{q}_n^i(k) = \left(\mathbf{I}_4 \cos \frac{\Delta\theta}{2} + \Delta\Theta \frac{\sin \frac{\Delta\theta}{2}}{\Delta\theta} \right) \mathbf{q}_n^i(k-1) \quad (29)$$

where

$$\begin{aligned} \Delta\theta &\approx \boldsymbol{\omega}_{in}^n \times T \\ &= [\boldsymbol{\omega}_{ie}^n + \mathbf{C}_b^n(t-1) \mathbf{F}_c (\mathbf{I}_3 - \boldsymbol{\phi}_m \times) (1 + \delta K) \mathbf{v}^m] \times T \\ &= [\Delta\theta_x \ \Delta\theta_y \ \Delta\theta_z]^T \end{aligned} \quad (30)$$

$$\Delta\theta = \sqrt{\Delta\theta_x^2 + \Delta\theta_y^2 + \Delta\theta_z^2} \quad (31)$$

$$\Delta\Theta = \begin{bmatrix} 0 & -\Delta\theta_x & -\Delta\theta_y & -\Delta\theta_z \\ \Delta\theta_x & 0 & \Delta\theta_z & -\Delta\theta_y \\ \Delta\theta_y & -\Delta\theta_z & 0 & \Delta\theta_x \\ \Delta\theta_z & \Delta\theta_y & -\Delta\theta_x & 0 \end{bmatrix} \quad (32)$$

Write the measurement model (17) as follows

$$\mathbf{y}_k = \boldsymbol{\alpha}_m(k) - \mathbf{C}_{n(k)}^i \boldsymbol{\beta}_m(k) = \mathbf{h}(\mathbf{X}_k) + \mathbf{V}_k \quad (33)$$

where \mathbf{V}_k is the measurement noise, which is assumed to be Gaussian process with zero means and covariance matrices \mathbf{R}_k . \mathbf{X}_k represents the ideal value of the filtering state at time instant k . $\mathbf{h}(\mathbf{X}_k)$ is the ideal measurement equation without noise and is a function related to \mathbf{X}_k .

The state estimation at time instant k is (25), and the corresponding covariance is $\mathbf{P}_{x,k}$, the RSRUSQUE algorithm for initial alignment is described as follows.

A. Time Update

Generate the sigma points as

$$\boldsymbol{\chi}_k(i) = \begin{cases} \hat{\mathbf{X}}_k, & i = 0 \\ \hat{\mathbf{X}}_k + [\sqrt{(n+\lambda)} \mathbf{S}_{x,k}]_i, & i = 1, 2, \dots, n \\ \hat{\mathbf{X}}_k - [\sqrt{(n+\lambda)} \mathbf{S}_{x,k}]_i, & i = n+1, n+2, \dots, 2n \end{cases} \quad (34)$$

where $\mathbf{S}_{x,k}$ is the lower triangular matrix obtained by using the Cholesky factorization of $\mathbf{P}_{x,k}$. n is the dimension of the state $\hat{\mathbf{X}}_k$, $\lambda = \sigma^2(n + \kappa) - n$. σ is a scale factor, usually a small quantity greater than zero, and its typical value range is $10^{-4} \leq \sigma \leq 1$, κ is a tuning parameter which is usually set to 0 and $3-n$ to capture some higher order information of the distribution. When the state dimension is greater than or equal to 3, κ takes 0, and when the state dimension is less than 3, κ takes $3-n$.

The weights corresponding to the expectation and covariance matrix is given by

$$W^m(i) = \begin{cases} \frac{\lambda}{n+\lambda}, & i = 0 \\ \frac{1}{2(n+\lambda)}, & i = 1, \dots, 2n \end{cases} \quad (35)$$

$$W^c(i) = \begin{cases} \frac{\lambda}{n+\lambda} + 1 - \sigma^2 + \varsigma, & i = 0 \\ \frac{1}{2(n+\lambda)}, & i = 1, \dots, 2n \end{cases} \quad (36)$$

where ς is used to incorporate prior information on the probability density function of the states. If it is a Gaussian distribution, then $\varsigma = 2$.

The sigma points $\boldsymbol{\chi}_k(i)$ can be divided into attitude part and non-attitude part, i.e.

$$\boldsymbol{\chi}_k(i) = [\boldsymbol{\chi}_k^{\delta\mathfrak{M}}(i)^T \ \boldsymbol{\chi}_k^e(i)^T]^T \quad (37)$$

The quaternion error corresponding to $\boldsymbol{\chi}_k^{\delta\mathfrak{M}}(i)$ is given by

$$\boldsymbol{\chi}_k^{\delta q}(i) = [\delta q_{k,0}(i) \ \delta \boldsymbol{\rho}_k(i)^T]^T \quad (38)$$

which can be calculated according to formula (28).

Define a new quaternion-based sigma point by multiplying the error quaternion by the current attitude quaternion

$$\boldsymbol{\chi}_k^q(i) = \boldsymbol{\chi}_k^{\delta q}(i) \otimes \mathbf{q}_k \quad (39)$$

Propagate these transformed sigma points through process model (29) and the propagated quaternion error is computed using

$$\boldsymbol{\chi}_{k+1|k}^{\delta q}(i) = \boldsymbol{\chi}_{k+1|k}^q(i) \otimes [\bar{\boldsymbol{\chi}}_{k+1|k}^q]^{-1} \quad (40)$$

$\bar{\boldsymbol{\chi}}_{k+1|k}^q$ is the average quaternion of the propagating quaternion sigma points, the explicit details about the $\bar{\boldsymbol{\chi}}_{k+1|k}^q$ can be referred in [35], [36].

Denote

$$\boldsymbol{\chi}_{k+1|k}^{\delta q}(i) = [\delta q_{k+1|k,0}(i) \ \delta \boldsymbol{\rho}_{k+1|k}(i)^T]^T \quad (41)$$

The predicted GRP sigma points corresponding to $\boldsymbol{\chi}_{k+1|k}^{\delta q}(i)$ can be calculated according to (27)

$$\boldsymbol{\chi}_{k+1|k}^{\delta\mathfrak{M}}(i) = \frac{\delta \boldsymbol{\rho}_{k+1|k}(i)}{1 + \delta q_{k+1|k,0}(i)} \quad (42)$$

The propagated sigma points of the state can now be determined as

$$\boldsymbol{\chi}_{k+1|k(i)} = [\boldsymbol{\chi}_{k+1|k}^{\delta\mathfrak{M}}(i)^T \ \boldsymbol{\chi}_{k+1|k}^e(i)^T]^T \quad (43)$$

The corresponding state prediction can be calculated through

$$\hat{\mathbf{X}}_{k+1|k} = \sum_{i=0}^{2n} W^m(i) \boldsymbol{\chi}_{k+1|k(i)} \quad (44)$$

The covariance is computed using a QR decomposition shown in (45) and a Cholesky factor update (downdate) of rank 1 shown in (46):

$$\begin{aligned} & \mathbf{S}_{x,k+1|k} \\ &= qr \left[\left[\sqrt{W^c(1:2n)} (\boldsymbol{\chi}_{k+1|k}(1:2n) - \hat{\mathbf{X}}_{k+1|k}) \sqrt{\mathbf{Q}_k} \right]^T \right] \end{aligned} \quad (45)$$

$$\begin{aligned} & \mathbf{S}_{x,k+1|k} \\ &= cholupdate \left\{ \mathbf{S}_{x,k+1|k}, \sqrt{|W^c(0)|} (\boldsymbol{\chi}_{k+1|k}(0) - \hat{\mathbf{X}}_{k+1|k}), \right. \\ & \quad \left. \text{sgn}(W^c(0)) \right\} \end{aligned} \quad (46)$$

Some details of QR decomposition and Cholesky factor update (downdate) are as follows:

QR decomposition: The QR decomposition of a matrix $\mathbf{A} \in \mathbb{R}^{N \times L}$ is given by, $\mathbf{A} = \mathbf{Q}\mathbf{R}$, where $\mathbf{Q} \in \mathbb{R}^{N \times N}$ is an orthogonal matrix, $\mathbf{R} \in \mathbb{R}^{N \times L}$ is an upper triangular

matrix. We use the shorthand notation $qr\{\cdot\}$ to denote a QR decomposition of a matrix where only R is returned.

Cholesky factor updating: Suppose that A has a Cholesky factorization of $\mathbf{R}^T \mathbf{R}$, R is an upper triangular matrix, then $cholupdate\{\mathbf{R}, \sqrt{\nu} \mathbf{x}, \pm\}$ is equivalent to finding the square root of $A \pm \nu \mathbf{x} \mathbf{x}^T$.

B. Measurement Update

Similar to (34), the state prediction $\hat{\mathbf{X}}_{k+1|k}$ and covariance $S_{x,k+1|k}$ are used to regenerate the sigma points $\mathbf{x}_{k+1|k}^*(i)$. Similar to (37)-(39), the new quaternion-based sigma points $\mathbf{x}_{k+1|k}^{*q}(i)$ can be obtained, and define a new set of sigma points as

$$\mathbf{y}_{k+1|k}^*(i) = [\mathbf{x}_{k+1|k}^{*q}(i)^T \mathbf{x}_{k+1|k}^{*e}(i)^T]^T \quad (47)$$

The propagated sigma points in (47) are propagated directly through the measurement model (33), the predicted sigma points as $\mathbf{Z}_{k+1|k}(i)$.

The mean of the measurements associated with each sigma point set can be calculated through

$$\hat{\mathbf{Y}}_{k+1} = \sum_{i=0}^{2n} W^m(i) \mathbf{Z}_{k+1|k}(i) \quad (48)$$

The covariance of the measurement and the cross-covariance of the state and measurement are given by

$$S_{y,k+1} = qr \left\{ \left[\sqrt{W^c(1:2n)} (\mathbf{Z}_{k+1|k}(1:2n) - \hat{\mathbf{Y}}_{k+1}) \sqrt{\mathbf{R}_k} \right]^T \right\} \quad (49)$$

$$S_{y,k+1} = cholupdate \left\{ S_{z,k+1}, \sqrt{|W^c(0)|} (\mathbf{Z}_{k+1|k}(0) - \hat{\mathbf{Y}}_{k+1}), \operatorname{sgn}(W^c(0)) \right\} \quad (50)$$

$$\begin{aligned} P_{xy,k+1} &= \sum_{i=0}^{2n} W^c(i) \left\{ (\mathbf{x}_{k+1|k}^*(i) - \hat{\mathbf{X}}_{k+1|k}) \right. \\ &\quad \times \left. (\mathbf{Z}_{k+1|k}(i) - \hat{\mathbf{Y}}_{k+1})^T \right\} \end{aligned} \quad (51)$$

The innovation vector is

$$\mathbf{e}_{k+1} = \mathbf{y}_{k+1} - \hat{\mathbf{Y}}_{k+1} \quad (52)$$

1) Adaptive Processing of Measurement Noise Covariance Matrices: Getting the variance on both sides of formula (52) simultaneously

$$\begin{aligned} E[\mathbf{e}_{k+1} \mathbf{e}_{k+1}^T] &= (\mathbf{h}(\mathbf{X}_{k+1}) + \mathbf{V}_{k+1} - \hat{\mathbf{Y}}_{k+1}) \\ &\quad \times (\mathbf{h}(\mathbf{X}_{k+1}) + \mathbf{V}_{k+1} - \hat{\mathbf{Y}}_{k+1})^T \\ &= (\mathbf{h}(\mathbf{X}_{k+1}) - \hat{\mathbf{Y}}_{k+1}) \\ &\quad \times (\mathbf{h}(\mathbf{X}_{k+1}) - \hat{\mathbf{Y}}_{k+1})^T + \mathbf{R}_{k+1} \end{aligned} \quad (53)$$

where

$$\begin{aligned} \mathbf{P}_{yy,k+1} &= (\mathbf{h}(\mathbf{X}_{k+1}) - \hat{\mathbf{Y}}_{k+1}) \times (\mathbf{h}(\mathbf{X}_{k+1}) - \hat{\mathbf{Y}}_{k+1})^T \\ &= \mathbf{S}_{y,k+1} \mathbf{S}_{y,k+1}^T - \mathbf{R}_k \end{aligned} \quad (54)$$

According to (53) and (54), the measurement noise covariance matrix \mathbf{R}_{k+1} is given by

$$\begin{aligned} \mathbf{R}_{k+1} &= E[\mathbf{e}_{k+1} \mathbf{e}_{k+1}^T] - \mathbf{S}_{y,k+1} \mathbf{S}_{y,k+1}^T + \mathbf{R}_k \\ &= \frac{1}{k} \sum_{i=1}^k (\mathbf{e}_{i+1} \mathbf{e}_{i+1}^T - \mathbf{S}_{y,i+1} \mathbf{S}_{y,i+1}^T + \mathbf{R}_i) \\ &= \frac{1}{k} \left[\sum_{i=1}^{k-1} (\mathbf{e}_{i+1} \mathbf{e}_{i+1}^T - \mathbf{S}_{y,i+1} \mathbf{S}_{y,i+1}^T + \mathbf{R}_i) \right. \\ &\quad \left. + (\mathbf{e}_{k+1} \mathbf{e}_{k+1}^T - \mathbf{S}_{y,k+1} \mathbf{S}_{y,k+1}^T + \mathbf{R}_k) \right] \\ &= \left(1 - \frac{1}{k}\right) \mathbf{R}_k + \frac{1}{k} (\mathbf{e}_{k+1} \mathbf{e}_{k+1}^T - \mathbf{S}_{y,k+1} \mathbf{S}_{y,k+1}^T + \mathbf{R}_k) \end{aligned} \quad (55)$$

It is known from (55) that the adaptive ability will be weakened after filtering for a long time, in order to maintain consistently the adaptive ability of the appropriate size, the formula (55) is improved as

$$\mathbf{R}_{k+1} = (1 - \eta_{k+1}) \mathbf{R}_k + \eta_{k+1} (\mathbf{e}_{k+1} \mathbf{e}_{k+1}^T - \mathbf{S}_{z,k+1} \mathbf{S}_{z,k+1}^T + \mathbf{R}_k) \quad (56)$$

$$\eta_{k+1} = \frac{\eta_k}{\eta_k + c} \quad (57)$$

where $\eta_0 = 1$, and $0 < c < 1$ is called fading factor, which is usually $c = 0.9 \sim 0.999$. If the measurement noise of the actual system is relatively small compared with the theoretical modeling value and the initial state noise setting is too large, \mathbf{R}_{k+1} will easily lose positive definiteness, which will cause abnormal filtering. An effective way to avoid this problem is to use sequential filtering method and limit the size of each element of \mathbf{R}_{k+1} diagonal. Set the lower limit condition $R_{\min}^{(i)}$ to ensure that \mathbf{R}_{k+1} is positive, and then use the upper limit condition $R_{\max}^{(i)}$ to quickly reduce the credibility of $y_{k+1}^{(i)}$. \mathbf{R}_{k+1} is a diagonal matrix, and the superscript (i) represents the i^{th} element of the matrix. The measurement noise covariance matrix can be written as

$$R_{k+1}^{(i)} = \begin{cases} (1 - \eta_{k+1}) R_k^{(i)} + \eta_{k+1} R_{\min}^{(i)} & p_{k+1}^{(i)} < R_{\min}^{(i)} \\ R_{\max}^{(i)} & p_{k+1}^{(i)} > R_{\max}^{(i)} \\ (1 - \eta_{k+1}) R_k^{(i)} + \eta_{k+1} p_{k+1}^{(i)} & \text{others} \end{cases} \quad (58)$$

$$p_{k+1}^{(i)} = e_{k+1}^{(i)} e_{k+1}^{(i)T} - S_{z,k+1}^{(i)} S_{z,k+1}^{(i)T} + R_k^{(i)} \quad (59)$$

Using (49)-(51), the update equations of the state vector and covariance matrix are determined by

$$\hat{\mathbf{X}}_{k+1} = \hat{\mathbf{X}}_{k+1|k} + \mathbf{P}_{xy,k+1} (\mathbf{S}_{y,k+1} \mathbf{S}_{y,k+1}^T)^{-1} \mathbf{e}_{k+1} \quad (60)$$

$$\mathbf{U}_{k+1} = \mathbf{P}_{xy,k+1} (\mathbf{S}_{y,k+1} \mathbf{S}_{y,k+1}^T)^{-1} \mathbf{S}_{y,k+1} \quad (61)$$

$$\mathbf{S}_{x,k+1} = cholupdate(\mathbf{S}_{x,k+1|k}, \mathbf{U}_{k+1}, -1) \quad (62)$$

2) Double Gain Processing: Most of the existing methods only use the priori measurement residuals of the current time step to complete the measurement update and state estimation, but ignore the utilization of the posteriori measurement residuals. In this part, the second gain matrix of posteriori measurement residuals are derived based on Kalman filter and the state vector and state covariance matrix are updated.

On the basis of robust estimated state vector and its covariance matrix, the state vector and state covariance matrix are further updated as the following equation

$$\hat{X}_{k+1}^* = \hat{X}_{k+1} + K_2 e_{k+1}^* \quad (63)$$

$$e_{k+1}^* = y_{k+1} - \hat{Y}_{k+1}^* \quad (64)$$

$$\begin{aligned} P_{x,k+1}^* &= S_{x,k+1}^* (S_{x,k+1}^*)^T \\ &= E \left[(x - \hat{X}_{k+1}^*) (x - \hat{X}_{k+1}^*)^T \right] \\ &= E \left[(x - \hat{X}_{k+1} - K_2 e_{k+1}^*) \right. \\ &\quad \left. (x - \hat{X}_{k+1} - K_2 e_{k+1}^*)^T \right] \\ &= E \left[(x - \hat{X}_{k+1}) (x - \hat{X}_{k+1})^T \right] \\ &\quad - E \left[(x - \hat{X}_{k+1}) (K_2 e_{k+1}^*)^T \right] \\ &\quad - E \left[(K_2 e_{k+1}^*) (x - \hat{X}_{k+1})^T \right] \\ &\quad + E \left[(K_2 e_{k+1}^*) (K_2 e_{k+1}^*)^T \right] \\ &= P_{x,k+1} - P_{xy,k+1}^* K_2 - K_2 (P_{xy,k+1}^*)^T \\ &\quad + K_2 P_{y,k+1}^* K_2^T \end{aligned} \quad (65)$$

where K_2 is the second gain matrix, $P_{x,k+1} = S_{x,k+1} S_{x,k+1}^T$, $P_{y,k+1}^* = S_{y,k+1}^* S_{y,k+1}$. The solution for \hat{Y}_{k+1}^* , $S_{y,k+1}$ and $P_{xy,k+1}^*$ are the same as for \hat{Y}_{k+1} , $S_{y,k+1}$ and $P_{xy,k+1}$, except that \hat{Y}_{k+1}^* uses \hat{X}_{k+1} and $S_{x,k+1}$ rather than $\hat{X}_{k+1|k}$ and $P_{x,k+1|k}$.

Because $P_{x,k+1}^*$ is a quadratic function of K_2 , the $P_{x,k+1}^*$ can be minimized with respect to K_2 . Setting it to zero, yields

$$\frac{\partial P_{x,k+1}^*}{\partial K_2} = -2P_{xy,k+1}^* + 2K_2 P_{y,k+1}^* = 0 \quad (66)$$

According to (62), the second gain matrix K_2 is

$$K_2 = P_{xy,k+1}^* P_{y,k+1}^{*-1} = P_{xy,k+1}^* \left(S_{y,k+1}^* S_{y,k+1}^{*T} \right)^{-1} \quad (67)$$

Substitute (63) into (61), (61) can be rewritten as

$$\begin{aligned} P_{x,k+1}^* &= P_{x,k+1} \\ &\quad - P_{xy,k+1}^* \left(P_{y,k+1}^{*-1T} + P_{y,k+1}^{*-1} \right. \\ &\quad \left. - P_{y,k+1}^{*-1} P_{y,k+1}^* P_{y,k+1}^{*-1T} \right) P_{xy,k+1}^* \\ &= P_{x,k+1} - P_{xy,k+1}^* P_{xy,k+1}^* P_{xy,k+1}^{*T} \end{aligned} \quad (68)$$

$$P^* = P_{y,k+1}^{*-1T} + P_{y,k+1}^{*-1} - P_{y,k+1}^{*-1} P_{y,k+1}^* P_{y,k+1}^{*-1T} \quad (69)$$

It can be known from (64) that $P_{x,k+1}^* \leq P_{x,k+1}$, so the filter with double gain structure has a faster convergence rate.

Using (63), (67), (68) and (69), the new state vector and new covariance matrix can be expressed as

$$\hat{X}_{k+1}^* = \hat{X}_{k+1} + P_{xy,k+1}^* \left(S_{y,k+1}^* S_{y,k+1}^{*T} \right)^{-1} e_{k+1}^* \quad (70)$$

$$U_{k+1}^* = P_{xy,k+1}^* \text{chol} (P^*)^T \quad (71)$$

$$S_{x,k+1}^* = \text{cholupdate} (S_{x,k+1}, U_{k+1}^*, -1) \quad (72)$$

where $\text{chol}(A) = R^T R$, R is an upper triangular matrix.

C. Attitude Update

The updated status vector is expressed as

$$\hat{X}_{k+1} = \hat{X}_{k+1}^* = [\delta \mathfrak{R}_{k+1}^T \ X_{k+1}^{eT}]^T \quad (73)$$

The quaternion error corresponding to $\delta \mathfrak{R}_{k+1}$ is given by

$$\delta q_{k+1} = [\delta q_{k+1,0} \ \delta \rho_{k+1}^T]^T \quad (74)$$

which can be calculated according to formula (28).

The attitude quaternion is updated through

$$q_{k+1} = \delta q_{k+1} \otimes \tilde{x}_{k+1|k}^q \quad (75)$$

Reset $\delta \mathfrak{R}_{k+1}$ to zeros and goes to the next filtering cycle.

At this point, the fast robust in-motion alignment for LDV-aided SINS has been implemented. For clarity, procedure of the proposed alignment method is illustrated in Table I.

D. Observability Analysis

Due to the scale factor error and installation misalignment angles of LDV are considered in the in-motion alignment, it is necessary to analyze the observability of these parameters to ensure the effectiveness of these parameters.

Considering that the purpose of filtering is to give state estimation, smaller state error corresponds to more accurate state estimation. And the variation degree of the diagonal elements of the state error covariance matrix with time describes the estimation effect of the corresponding state components. If the diagonal elements of the state error covariance matrix change significantly compared with the initial value, the corresponding state component can be considered to have high observability. Therefore, in this paper, the observability of each component $\hat{X}_{k+1(j)}$ in the state vector can be described as follows

$$O_{k+1(j)} = \sqrt{\frac{\mathbf{P}_{0(jj)}}{\left(S_{x,k+1(j)}^* \right)^T S_{x,k+1(j)}^*}} \quad (76)$$

where \mathbf{P}_0 represents initial state estimation covariance matrix.

According to practical experience, if $O_{k+1(j)} > 10$, indicating that the $\hat{X}_{k+1(j)}$ has strong observability, if $O_{k+1(j)} \leq 1$, indicating that the $\hat{X}_{k+1(j)}$ is not observable.

IV. VEHICLE-MOUNTED FIELD TEST

Two groups of vehicle-mounted tests were carried out to evaluate the superior performance of the proposed alignment method. In the test, a self-developed IMU, a dual-antenna GPS receiver, a navigation computer and a self-made LDV are equipped on the car, as shown in Fig. 1. The IMU consists of

TABLE I
FAST ROBUST IN-MOTION ALIGNMENT FOR LDV-AIDED SINS

$$\text{Initialization: } \alpha_m(0) = \beta_m(0) = \theta, C_b^n(0) = C_{n(0)}^i = C_{b(0)}^i = I_3, \delta K = 0$$

$$q_0 = \delta q_0 = [1 \ 0 \ 0 \ 0]^T, Q_k = \text{diag}([10^{-7} \ 10^{-7} \ 10^{-7} \ 0 \ 0 \ 0]^T)^2$$

$$R_0 = \text{diag}([0.07 \ 0.07 \ 0.07]^T)^2, C_m^b(0) = I_3$$

$$S_{x,0} = \text{diag}\left(\left[\frac{\pi}{60} \ \frac{\pi}{60} \ \frac{\pi}{15} \ 0.1^\circ \ 0.02^\circ \ 0.009\right]^T\right)$$

Inputs: $\omega_{ib}^b(t_k), f^b(t_k), v^m(t_k)$.

Construct process model and measurement model:

Update $C_{b(t_{k+1})}^i$ and $C_{n(t_{k+1})}^i$ using (8) and (18), and the (18) is the process model.

The measurement model is constructed through (17), the $\alpha_m(t)$ and $\beta_m(t)$ in (17) calculated according to (20)-(24).

Perform the filtering process:

Time update:

Determination filtering state vector \hat{X}_k by (25)-(27).

Generate the sigma points $\chi_k(i)$ according to (25) and (34).

Calculate propagated sigma points of the state $\chi_{k+1|k}(i)$ by (42) and (43).

Calculate corresponding state prediction $\hat{X}_{k+1|k}$ and the square root form of the prediction covariance $S_{x,k+1|k}$ by (44)-(46).

Measurement update:

Calculate the predicted sigma points of the measurement $Z_{k+1|k}(i)$ by (33) and (47).

Calculate the mean of the measurements \hat{Y}_{k+1} and the square root form of the covariance of the measurement $S_{y,k+1}$ and the cross-covariance of the state and measurement $P_{xy,k+1}$ by (48)-(51).

The measurement noise covariance matrix R_{k+1} is adaptive processed by (53)-(59).

Calculate the state vector \hat{X}_{k+1} and the square root form of the state covariance $S_{x,k+1}$ by (49)-(51) and (60)-(61).

Calculate the second gain matrix K_2 and update the state vector \hat{X}_{k+1}^* and the square root form of the state covariance $S_{x,k+1}^*$ by (67)-(72).

Attitude update:

Update the attitude quaternion q_{k+1} through (73)-(75).

Calculate $C_b^n(t_{k+1})$:

Calculate $C_b^n(t_{k+1})$ using $C_b^n(t_{k+1}) = C_i^{n(t_{k+1})} C_{b(t_{k+1})}^i$, and $C_i^{n(t_{k+1})}$ can be obtained from q_{k+1} , $C_{b(t_{k+1})}^i$ can be obtained by (8).

Calculate $C_{b(0)}^{n(0)}$ using $C_{b(0)}^{n(0)} = C_{n(t_{k+1})}^{n(0)} C_i^{n(t_{k+1})}$.

Reset δR_{k+1} to zeros and goes to the next cycle.

Output: $C_b^n(t_{k+1}), \delta K, \phi_{mx}, \phi_{mz}$.

three ring laser gyroscopes and three quartz accelerometers. The bias instability of the gyroscopes is within $0.008^\circ/\text{h}$, the random walk of the gyroscopes is within $0.003^\circ/\sqrt{\text{h}}$, the bias instability of the accelerometers is within $50\mu\text{g}$, the random walk of the accelerometers is $50\mu\text{g}/\sqrt{\text{h}}$, and the velocity measurement error of the LDV is $0.1\%(\sigma)$. The data output frequency of the IMU and LDV is 100 Hz. The horizontal positioning accuracy and the altitude accuracy of the GPS are within 0.05m, and its data output frequency is 10 Hz.



Fig. 1. Installation diagram of the experimental system.

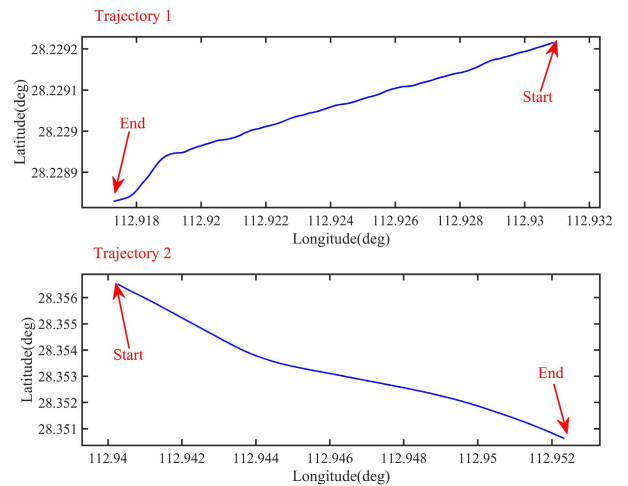


Fig. 2. Trajectory of the vehicle in the field test.

Two groups of field tests were performed in Changsha City. Firstly, the vehicle remains stationary at the start point for about 13 minutes and the static attitude alignment was performed to obtain the accurate initial attitude. Considering that the initial conditions are very accurate, and the SINS/GPS integrated navigation system output accuracy in attitude estimation is related to the external environment and vehicle maneuvering, so, the attitude obtained by static attitude alignment is used as the reference attitude to evaluate the alignment method. The movement trajectories are shown in Fig. 2. The outputs of LDV are shown in Fig. 3, where the second group of data is disturbed by noise.

In order to evaluate the alignment performance of the proposed scheme, the following five initial alignment schemes are designed for comparison.

Scheme 1: An OBA method, which is proposed in [13]

Scheme 2: A USQUE method, which is proposed in [20]

Scheme 3: Based on *Scheme 2*, the measurement noise covariance matrix is adaptively processed

Scheme 4: Based on *Scheme 5*, double gain structure, LDV installation error and LDV scale factor are ignored

Scheme 5: RDGSR-USQUE method proposed in this paper

In each test group, the initial value of attitude quaternion are all set as $[1 \ 0 \ 0 \ 0]^T$ for four schemes. For *Scheme 2*, *Scheme 3*, *Scheme 4* and *Scheme 5*, the initial covariance

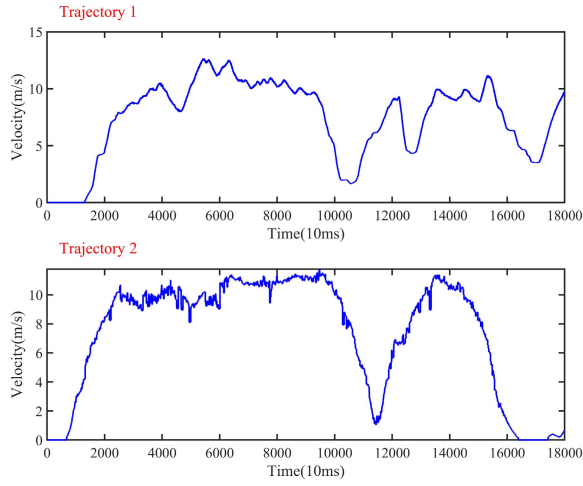


Fig. 3. Velocity curve of LDV output.

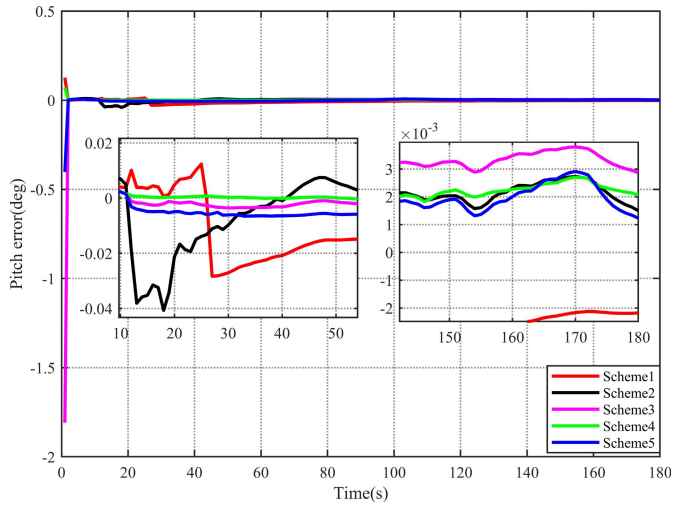


Fig. 4. Pitch angle errors by different schemes in trajectory 1.

matrix of attitude error are set as $\text{diag}([3^\circ \ 3^\circ \ 12^\circ]^T)^2$. For *Scheme 4*, the initial covariance matrix of LDV related error terms is set as $\text{diag}([0.1^\circ \ 0.02^\circ \ 0.009]^T)$. The attitude errors of different schemes in different trajectories are shown in Figs. 4-9. The LDV installation misalignment angle and scale factor estimation by *Scheme 5* in two trajectories are shown in Figs. 10-11.

In Figs. 4-6 and Figs. 10, the superiority of *Scheme 5* is obvious compared with other schemes, and *Scheme 5* can estimate the installation misalignment angle and scale factor of LDV at the same time of alignment, whereas the other four schemes cannot provide these errors. The alignment results show that the accuracy of the pitch angle of the five schemes is approximately equivalent, but the accuracy of the roll angle and heading angle of *Scheme 5* is better than the other four schemes. In the first group of field test, the attitude error by *Scheme 5* at the end of alignment is 0.0012° , -0.0029° , and 0.0756° for pitch, roll and heading, respectively. Additionally, among the estimates from all angles, *Scheme 5* has the optimal convergence speed and stability. The comparison between

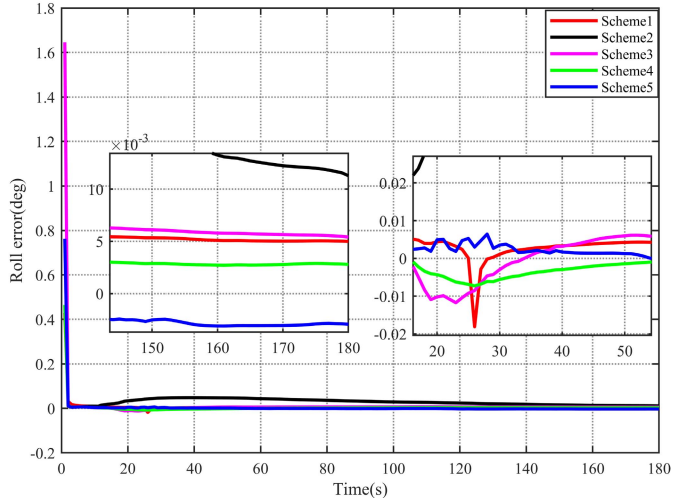


Fig. 5. Roll angle errors by different schemes in trajectory 1.

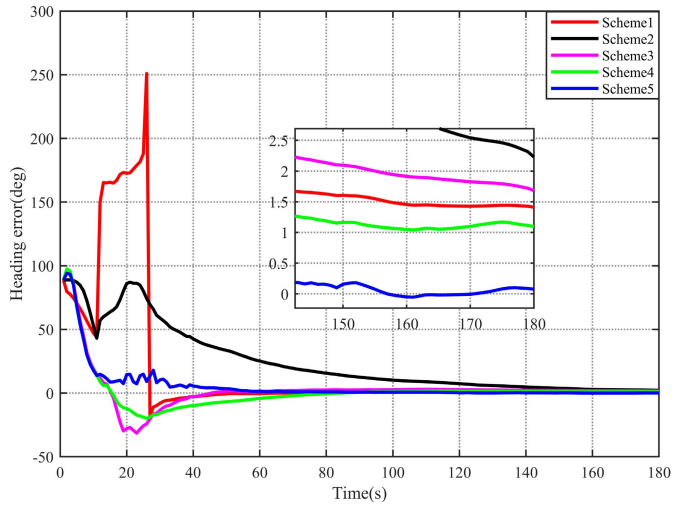


Fig. 6. Heading angle errors by different schemes in trajectory 1.

Scheme 5 and *Scheme 1*, *Scheme 2* shows that effective noise suppression and the consideration of unknown parameter errors can improve the alignment accuracy and alignment speed. The comparison between *Scheme 3* and *Scheme 2* and *Scheme 4* and *Scheme 3* shows that adaptive filtering and double gain processing can improve the alignment accuracy. Comparing *Scheme 5* with *Scheme 4*, it shows that it is helpful to improve the accuracy and convergence speed of alignment by considering and estimating the installation misalignment angle and scale factor of LDV in the process of alignment and use double gain structure.

In order to test the robustness of the proposed scheme, the threshold of LDV was adjusted in the second set of vehicle tests, so that LDV cannot filter the noise signal effectively. It can be seen from Figs. 7-9 and Fig. 11 that the alignment accuracy and convergence speed of the four schemes are weakened under noise interference, but *Scheme 5*, *Scheme 4* and *Scheme 3* have better robustness and alignment accuracy than *Scheme 1* and *Scheme 2*. Although the estimation accuracy of installation misalignment angle and scale factor of LDV

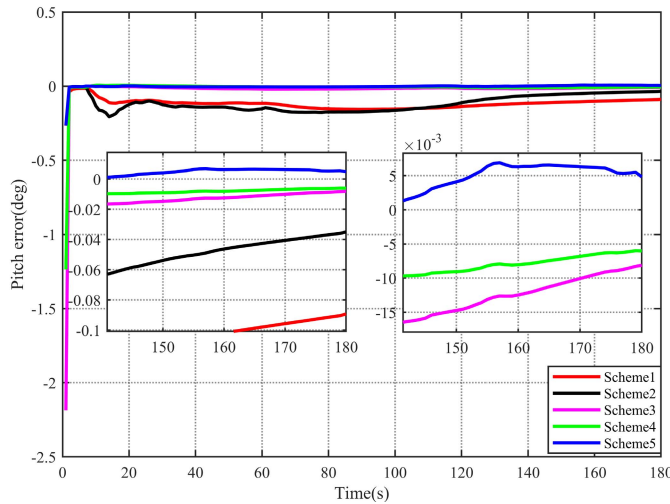


Fig. 7. Pitch angle errors by different schemes in trajectory 2.

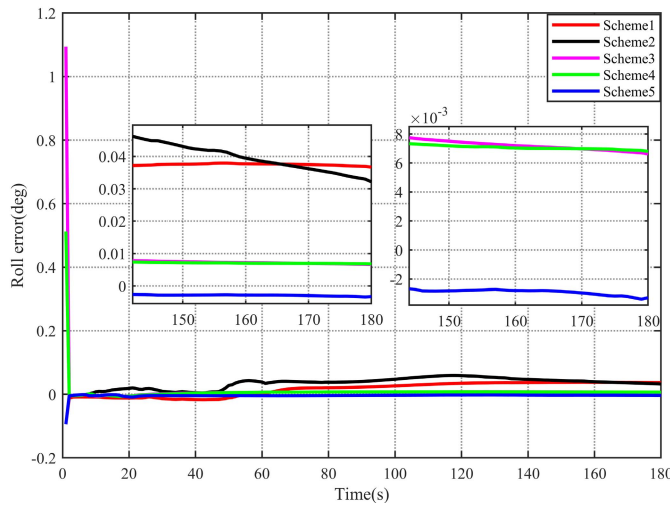


Fig. 8. Roll angle errors by different schemes in trajectory 2.

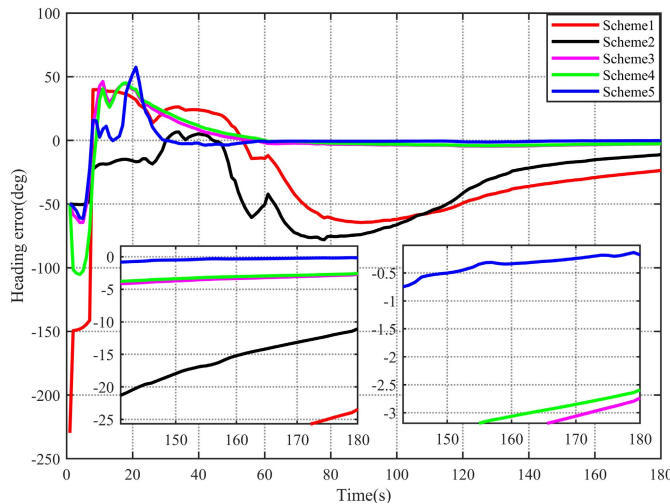


Fig. 9. Heading angle errors by different schemes in trajectory 2.

decreases under the interference of noise, *Scheme 5* still keeps higher alignment accuracy and faster alignment speed than *Scheme 4*. In the second group of field test, the attitude error

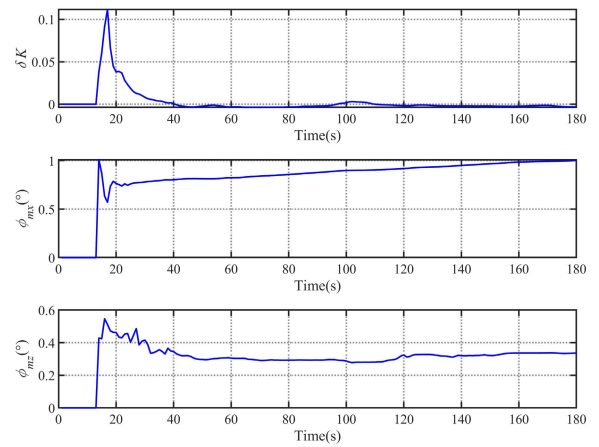


Fig. 10. Curves of LDV related parameters in trajectory 1.

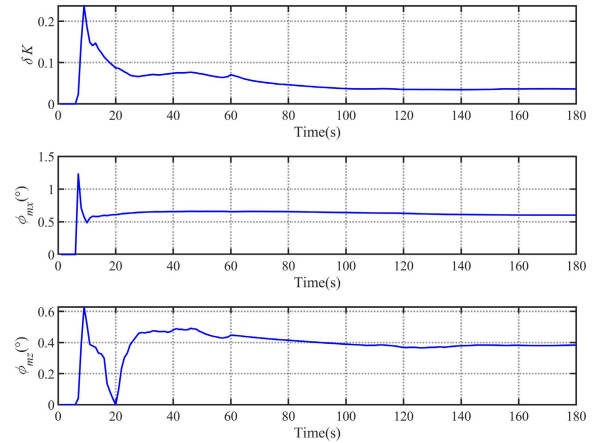


Fig. 11. Curves of LDV related parameters in trajectory 2.

TABLE II
STATISTICS OF THE HEADING ANGLE ERRORS
OF VEHICLE IN THE FIRST GROUP TEST

	Time(s)	31~90	91~150	151~180
<i>Scheme 1</i>	Mean	-0.8428	1.5844	1.4680
	STD	1.8883	0.2176	0.0561
<i>Scheme 2</i>	Mean	27.9298	7.4411	2.8038
	STD	12.3834	2.4510	0.4193
<i>Scheme 3</i>	Mean	0.1794	2.5757	1.8775
	STD	3.4721	0.2659	0.1026
<i>Scheme 4</i>	Mean	-4.9062	1.3816	1.1009
	STD	4.2753	0.2376	0.0425
<i>Scheme 5</i>	Mean	2.5767	0.3855	0.0359
	STD	2.2173	0.2229	0.0457

by *Scheme 5* at the end of alignment is 0.0048° , -0.0032° , and -0.1760° for pitch, roll, and heading, respectively.

In order to compare the alignment performance of the four schemes more specifically, the mean and standard deviation are compared. The statistics are shown in Table II-III.

It can be seen from Table II that the mean of the heading angle errors of *Scheme 5* are the smallest between 90 and 180s, which shows that *Scheme 5* has faster convergence speed than other schemes. During the period of 31-180s, the standard

TABLE III
STATISTICS OF THE HEADING ANGLE ERRORS OF
VEHICLE IN THE SECOND GROUP TEST

	Time(s)	31~90	91~150	151~180
<i>Scheme 1</i>	Mean	-18.2930	-48.7706	-27.6657
	STD	35.0209	10.8812	2.5624
<i>Scheme 2</i>	Mean	-43.7035	-42.7654	-14.2077
	STD	32.9582	18.7315	1.9471
<i>Scheme 3</i>	Mean	1.5692	-3.9584	-3.1946
	STD	5.9335	0.3901	0.2661
<i>Scheme 4</i>	Mean	3.4539	-3.5832	-2.9524
	STD	6.7275	0.3977	0.2089
<i>Scheme 5</i>	Mean	-1.4999	-0.8392	-0.2843
	STD	1.0528	0.2617	0.0686

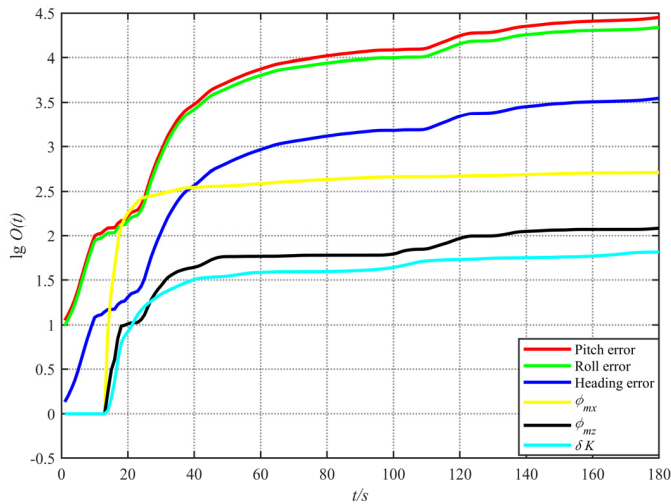


Fig. 12. Curves of state observability in trajectory 1.

deviations of the heading angle error of *Scheme 5* are almost the smallest, illustrating that the proposed method has good stability. Considering the mean and standard deviation, *Scheme 5* has better performance than other schemes. It can be seen from Table III that when the output of LDV is no longer accurate enough, the advantage of *Scheme 5* is more significant according to the analysis of mean and standard deviation. It can still complete the alignment when other schemes are unable to alignment, but it takes more time to converge to higher accuracy. To sum up, *Scheme 5* is more suitable for in-motion alignment than other schemes.

In order to further verify the effectiveness of the proposed in-motion alignment method, the observability analysis is conducted on attitude error angle, LDV scale factor error and LDV installation misalignment angles, the logarithmic curve of observability of state are shown in Figs. 12-13.

It can be seen from Figs. 12-13 that although the observability of the three error parameters of LDV is not as good as attitude error angles of SINS, they still have strong observability. Therefore, in the alignment process, the in-motion alignment method proposed in this paper can effectively estimate the error parameters of LDV, which indicates that considering the LDV errors in the in-motion alignment process is beneficial to improve the alignment performance. In addition, it is also

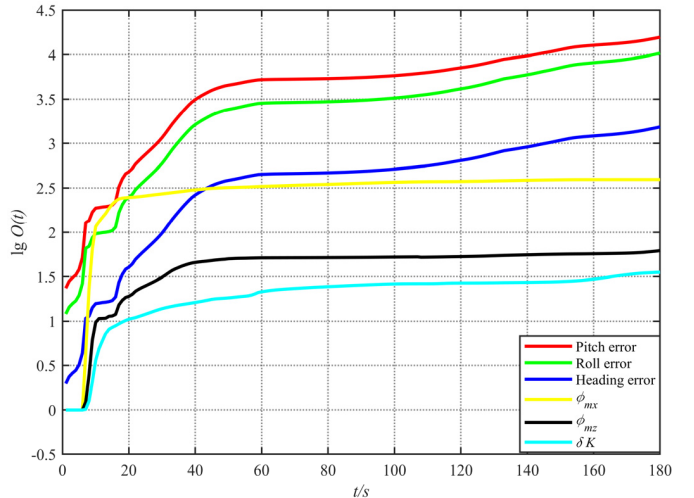


Fig. 13. Curves of state observability in trajectory 2.

beneficial to subsequent navigation when LDV errors estimated in the in-motion alignment.

V. CONCLUSION

This paper presents a novel RDGSR-USQUE method based on attitude estimation to realize the fast in-motion initial alignment for LDV-aided SINS aiming at weakening the effects of the installation misalignment angles between IMU and LDV and the scale factor error of LDV on alignment. RDGSR-USQUE method improves the defects of the traditional USQUE method, such as poor noise resistance, slow convergence speed under large misalignment angle and easy to lead to non-positive definite covariance matrix. This will help to estimate and compensate unknown parameter errors while estimating attitude, so as to improve the accuracy of process model and measurement model, and finally improve the accuracy of attitude estimation. Two groups of vehicle field tests were carried out to evaluate the performance of the proposed scheme. Experimental results show that the proposed scheme has higher alignment accuracy, faster convergence speed and stronger robustness than the other three schemes. In addition, this method also estimates the installation misalignment angles and scale factor of LDV installation satisfactorily, which will be beneficial to further calibration of LDV and improve the accuracy of integrated navigation.

REFERENCES

- [1] J. Fang and Z. Liu, "In-flight alignment of POS based on state-transition matrix," *IEEE Sensors J.*, vol. 15, no. 6, pp. 3258–3264, Jun. 2015.
- [2] Y. Wu and X. Pan, "Velocity/position integration formula—Part II: Application to strapdown inertial navigation computation," *IEEE Trans. Aerosp. Electron. Syst.*, vol. 49, no. 2, pp. 1024–1034, Apr. 2013.
- [3] Q. Wang, C. Gao, J. Zhou, G. Wei, X. Nie, and X. Long, "Two-dimensional laser Doppler velocimeter and its integrated navigation with a strapdown inertial navigation system," *Appl. Opt.*, vol. 57, no. 13, pp. 3334–3339, May 2018.
- [4] D. H. Titterton, J. L. Weston, and J. L. Weston, *Strapdown Inertial Navigation Technology*. London, U.K.: Peter Peregrinus Limited, 1997.
- [5] M. Liu, G. Li, Y. Gao, S. Li, and L. Guan, "Velocity-aided in-motion alignment for SINS based on pseudo-Earth frame," *J. Navigat.*, vol. 71, no. 1, pp. 221–240, Jan. 2018.

- [6] P. B. Davenport, "A vector approach to the algebra of rotations with applications," NASA, Washington, DC, USA, Tech. Rep. NASA TN D-4696, Aug. 1968.
- [7] M. Wu, Y. Wu, X. Hu, and D. Hu, "Optimization-based alignment for inertial navigation systems: Theory and algorithm," *Aerospace Sci. Technol.*, vol. 15, no. 1, pp. 1–17, Jan./Feb. 2011.
- [8] Y. Wu and X. Pan, "Velocity/position integration formula—Part I: Application to in-flight coarse alignment," *IEEE Trans. Aerospace Electron. Syst.*, vol. 49, no. 2, pp. 1006–1023, Apr. 2013.
- [9] Q. Zhang, S. Li, Z. Xu, and X. Niu, "Velocity-based optimization-based alignment (VBOBA) of low-end MEMS IMU/GNSS for low dynamic applications," *IEEE Sensors J.*, vol. 20, no. 10, pp. 5527–5539, May 2020.
- [10] X. Xu, D. Xu, T. Zhang, and H. Zhao, "In-motion coarse alignment method for SINS/GPS using position Loci," *IEEE Sensors J.*, vol. 19, no. 10, pp. 3930–3938, Jan. 2019.
- [11] L. Chang, J. Li, and K. Li, "Optimization-based alignment for strapdown inertial navigation system: Comparison and extension," *IEEE Trans. Aerospace Electron. Syst.*, vol. 52, no. 4, pp. 1697–1713, Aug. 2016.
- [12] L. Luo, Y. Huang, Z. Zhang, and Y. Zhang, "A position loci-based in-motion initial alignment method for low-cost attitude and heading reference system," *IEEE Trans. Instrum. Meas.*, vol. 70, pp. 1–18, 2021.
- [13] Y. Zhang, L. Luo, T. Fang, N. Li, and G. Q. Wang, "An improved coarse alignment algorithm for odometer-aided SINS based on the optimization design method," *Sensors*, vol. 18, no. 1, p. 195, Jan. 2018.
- [14] L. Kang, L. Ye, and K. Song, "A fast in-motion alignment algorithm for DVL aided SINS," *Math. Problems Eng.*, vol. 2014, pp. 1–12, Jun. 2014.
- [15] Y. Huang, Y. Zhang, and X. Wang, "Kalman-filtering-based in-motion coarse alignment for odometer-aided SINS," *IEEE Trans. Instrum. Meas.*, vol. 66, no. 12, pp. 3364–3377, Dec. 2017.
- [16] L. Luo, Y. Huang, Z. Zhang, and Y. Zhang, "A new Kalman filter-based in-motion initial alignment method for DVL-aided low-cost SINS," *IEEE Trans. Veh. Technol.*, vol. 70, no. 1, pp. 331–343, Jan. 2021.
- [17] W. Li, J. Wang, L. Lu, and W. Wu, "A novel scheme for DVL-aided SINS in-motion alignment using UKF techniques," *Sensors*, vol. 13, no. 1, pp. 1046–1063, Jan. 2013.
- [18] J. L. Crassidis and F. L. Markley, "Unscented filtering for spacecraft attitude estimation," *J. Guid., Control, Dyn.*, vol. 26, no. 4, pp. 536–542, Jul. 2003.
- [19] Y. Huang, Y. Zhang, and L. Chang, "A new fast in-motion coarse alignment method for GPS-aided low-cost SINS," *IEEE/ASME Trans. Mechatronics*, vol. 23, no. 3, pp. 1303–1313, Jun. 2018.
- [20] L. Chang, H. He, and F. Qin, "In-motion initial alignment for odometer-aided strapdown inertial navigation system based on attitude estimation," *IEEE Sensors J.*, vol. 17, no. 3, pp. 766–773, Feb. 2017.
- [21] L. Chang, Y. Li, and B. Xue, "Initial alignment for a Doppler velocity log-aided strapdown inertial navigation system with limited information," *IEEE/ASME Trans. Mechatronics*, vol. 22, no. 1, pp. 329–338, Feb. 2017.
- [22] L. Chang, J. Di, and F. Qin, "Inertial-based integration with transformed INS mechanization in Earth frame," *IEEE/ASME Trans. Mechatronics*, vol. 27, no. 3, pp. 1738–1749, Jun. 2022.
- [23] L. Chang, F. Qin, and J. Xu, "Strapdown inertial navigation system initial alignment based on group of double direct spatial isometries," *IEEE Sensors J.*, vol. 22, no. 1, pp. 803–818, Jan. 2022.
- [24] H. Xue, X. Guo, Z. Zhou, and K. Wang, "Motion alignment algorithm for vehicle carried SINS based on odometer aiding," *J. Navigat.*, vol. 70, no. 6, pp. 1349–1366, Jun. 2017.
- [25] Z. Jian and L. Xingwu, "Research on laser Doppler velocimeter for vehicle self-contained inertial navigation system," *Opt. Laser Technol.*, vol. 42, no. 3, pp. 477–483, 2010.
- [26] J. Zhou, "Research on multipoint layer-type laser Doppler self-velocimeter," *Opt. Eng.*, vol. 49, no. 4, Apr. 2010, Art. no. 044301.
- [27] J. Zhou, X. Nie, and J. Lin, "A novel laser Doppler velocimeter and its integrated navigation system with strapdown inertial navigation," *Opt. Laser Technol.*, vol. 64, pp. 319–323, Dec. 2014.
- [28] Q. Wang, X. Nie, C. Gao, J. Zhou, G. Wei, and X. Long, "Calibration of a three-dimensional laser Doppler velocimeter in a land integrated navigation system," *Appl. Opt.*, vol. 57, no. 29, pp. 8566–8572, Oct. 2018.
- [29] X. Nie and J. Zhou, "Pitch independent vehicle-based laser Doppler velocimeter," *Opt. Lasers Eng.*, vol. 131, Aug. 2020, Art. no. 106072.
- [30] R. Huang, Q. Wang, X. Nie, and J. Zhou, "One-dimensional reference-beam LDV for accurate altitude estimation in a land vehicle," *Appl. Opt.*, vol. 59, no. 34, pp. 10667–10672, Dec. 2020.
- [31] K. Tang, J. Wang, W. Li, and W. Wu, "A novel INS and Doppler sensors calibration method for long range underwater vehicle navigation," *Sensors*, vol. 13, no. 11, pp. 14583–14600, Oct. 2013.
- [32] M. Shuster, "A survey of attitude representations," *J. Astron. Sci.*, vol. 41, no. 4, pp. 439–517, Oct. 1993.
- [33] H. Schaub and J. L. Junkins, "Stereographic orientation parameters for attitude dynamics: A generalization of the Rodrigues parameters," *J. Astronaut. Sci.*, vol. 44, no. 1, pp. 1–19, Jan. 1995.
- [34] F. L. Markley, "Attitude error representations for Kalman filtering," *J. Guid., Control, Dyn.*, vol. 26, no. 2, pp. 311–317, 2003.
- [35] L. Chang, B. Hu, and G. Chang, "Modified unscented quaternion estimator based on quaternion averaging," *J. Guid. Control. Dyn.*, vol. 37, no. 1, pp. 305–308, Feb. 2014.
- [36] F. L. Markley, Y. Cheng, J. L. Crassidis, and Y. Oshman, "Averaging quaternions," *J. Guid., Control, Dyn.*, vol. 30, no. 4, pp. 1193–1197, 2007.

Zhiyi Xiang received the M.E. degree from the College of Advanced Interdisciplinary Studies, National University of Defense Technology, China, in 2021, where he is currently pursuing the Ph.D. degree. His current research interest is SINS/LDV integrated navigation technology.

Qi Wang received the M.E. degree from the College of Optoelectronic Science and Engineering, National University of Defense Technology, China, in 2013, and the Ph.D. degree from the College of Advanced Interdisciplinary Studies, National University of Defense Technology, in 2018.

He is currently a Lecturer with the College of Advanced Interdisciplinary Studies, National University of Defense Technology. His research interests include the laser Doppler velocimetry and SINS/LDV integrated navigation technology.

Rong Huang received the M.E. degree from the College of Advanced Interdisciplinary Studies, National University of Defense Technology, China, in 2019, where she is currently pursuing the Ph.D. degree. Her current research interests include the laser Doppler velocimetry and SINS/LDV integrated navigation technology.

Chongbin Xi received the M.E. degree from the College of Advanced Interdisciplinary Studies, National University of Defense Technology, China, in 2020, where he is currently pursuing the Ph.D. degree. His current research interest is SINS/LDV integrated navigation technology.

Xiaoming Nie received the M.E. degree from the College of Optoelectronic Science and Engineering, National University of Defense Technology, China, in 2010, and the Ph.D. degree from the College of Advanced Interdisciplinary Studies, National University of Defense Technology, in 2014.

He is currently a Lecturer with the College of Advanced Interdisciplinary Studies, National University of Defense Technology. His research interests include the optoelectronic velocimetry, laser Doppler velocimetry, and SINS/LDV integrated navigation technology.

Jian Zhou received the B.E. degree from the College of Optoelectronic Science and Engineering, National University of Defense Technology, China, in 2006, and the Ph.D. degree from the College of Advanced Interdisciplinary Studies, National University of Defense Technology, in 2011.

He is currently an Associate Professor with the College of Advanced Interdisciplinary Studies, National University of Defense Technology. His research interests include the optoelectronic velocimetry, laser Doppler velocimetry, and SINS/LDV integrated navigation technology.